Adhesive bonding of a mixed short and continuous carbon-fiber-reinforced Nylon-6 composite made via fused filament fabrication

M. Pizzorni [a,b,*], A. Parmiggiani [c], M. Prato [b]

[a] Department of Mechanical Engineering, Polytechnic School, University of Genoa, Via All'Opera Pia 15, 16145, Genoa, Italy
[b] Materials Characterization Facility, Istituto Italiano di Tecnologia, Via Morego 30, 16163, Genoa, Italy
[c] Mechanical Workshop Facility, Istituto Italiano di Tecnologia, Via al Santuario di Nostra Signora della Guardia 26B/R, 16162, Genoa, Italy

ARTICLE INFO

Keywords:
Carbon fiber reinforced thermoplastic
Additive manufacturing
Adhesive bonding
Failure analysis

ABSTRACT

This experimental work aims at evaluating the mechanical and failure behavior of adhesive-bonded single-lap joints made of a thermoplastic composite 3D-printed *via* Fused Filament Fabrication technology. Carbon fiber was selected as the reinforcement and used in the form of both short and continuous fibers embedded in the Nylon-6 matrix, forming the composite's hybrid structure. An approach based on progressive improvement of surface treatment effectiveness (solvent degreasing, abrasion, and low-pressure plasma) has been adopted to verify how the additively-manufactured composite responds to bonding when increased interfacial adhesion is attained by preparing the outer printed layer. Roughness measurements, wettability evaluations, and XPS analyses have been carried out to assess any modifications of morphology and functionalization exhibited by the different surfaces after treatment. The experimental findings demonstrate that the intrinsic non-homogeneity of 3D-printed composites is emphasized when low-pressure plasma is used, as it generates interfacial bonds between adhesive and adherend that are more effective than the interlaminar ones within the substrate. In this condition, the ultimate resistance of the joint corresponds to that of the base material. In particular, fracture-mechanism analysis allowed precise identification of the crack path, highlighting defects and current limitations of the additively-manufactured system and suggesting pivotal aspects to develop in future work to improve joint performance.

1. Introduction

In recent years, additive manufacturing (AM) of composite structures has been garnering increased interest among researchers and developers. This advance is related to the possibility of combining the wide range of composite materials available today with a manufacturing process that allows great freedom in the design and customization of the components.

AM is defined as the process of creating components by depositing material layer upon layer, starting from digital 3D model data. Thus, as opposed to subtractive methodologies, AM presents two fundamental features: direct manufacturing and layer-wise processing. Among all the AM technologies for fabricating polymer components, Fused Filament Fabrication (FFF) is widely diffused. FFF is advantageous thanks to its process flexibility, robustness and reliability, low material wastage and relatively low cost of printers and consumables [1]. These factors have led to a progressive technological evolution that allowed new challenges to be faced and different fields of application.

In this scenario, 3D printing of thermoplastic-polymer composites is becoming a more and more promising solution for turning AM from a prototyping technology to a fabrication process to be implemented for real-world applications. Over time, the developments in additive technologies have accompanied the evolution of the materials processable, progressively allowing the filling of thermoplastic filaments, such as Nylon, PLA, ABS, PEEK, with various filler-type reinforcements, such as short fibers including chopped carbon fibers [2], glass fibers [3], carbon nanotubes [4], to name a few. With the most recent technologies available, the use of continuous fibers (CF) – such as glass, carbon, or Kevlar [5] – has allowed an extra potential in functional parts with a substantial effect on the mechanical properties [6]: with these composites, maximum stiffness and strength can be achieved, since most of the load is borne by the CF oriented along the load direction. In this context, AM Carbon Fiber Reinforced Thermoplastic (CFRT) composites are becoming particularly attractive, since they exhibit superior

* Corresponding author. Department of Mechanical Engineering, Polytechnic School, University of Genoa, Via All'Opera Pia 15, 16145, Genoa, Italy.
E-mail address: marco.pizzorni@dime.unige.it (M. Pizzorni).

mechanical strength, stiffness, recyclability, and the potential for light-weight structures, that may even enable them to become substitute materials for the more conventional thermosetting polymers.

Following the technological advances, several industries, including aerospace, automotive, or robotics, are pushing AM as an alternative method for the production of their composite components. AM of CF composites, however, represents a relatively new technique, and finding adequate solutions for the design and modeling of such printed structures is not always easy. As also recently pointed out by Kabir et al. [7], indeed, there is still a lack of research on aspects that may be equally helpful to understand to what extent AM-CFRT materials can be used and what challenges remain. Firstly, to be considered as valid alternatives to the more traditional polymer composites, AM CFRT materials have to satisfy similar performance requirements, needing in-depth optimization of the construction criteria, specifically of the process parameters that dictate the final quality of the 3D-printed part. Concerning this, several efforts have been (and are being) made to identify proper printing methods (and related parameters) for the fabrication of such materials [8–13].

To date, two systems employing fiber-laydown methods are available: the first is based on the deposition of fibers by using a 6-DOF robot arm (e.g., Continuous Composites, Moi Composites); the second performs deposition of fiber-reinforced plastics through a standard desktop 3D printer (e.g., Markforged, Anisoprint, Desktop Metal). This work concentrates on the latter, which are most commonly used thanks to their relative ease of use, precision, and small size. However, desktop printers' built volume inevitably limits the built-component dimension, making it usual that the final product might be realized by joining several additively-manufactured smaller parts. Alternatively, printed components, built to replace damaged components, might need to be joined to pre-existing parts. As a consequence, the design criteria at the basis of 3D-printing of composite components have to follow a 'building-block' approach, causing assembly operations to have to be integrated into the manufacturing process.

Among the joining methods for pure or reinforced plastics, adhesive bonding is recognized as the least invasive today, ensuring excellent mechanical performance and guaranteeing high quality in different operative conditions [14]. In the specific case of plastic composites, adhesive joining has significant advantages over mechanical joining methods, since the adhesive layer yields a continuous bond between the substrates, reducing residual stresses and acting as a mechanical buffer to absorb energy during impacts. Nevertheless, obtaining proper features is not straightforward. Indeed, adhesive bonding requires an accurate design of the entire process, which should involve geometric evaluations of the areas to be joined, the choice of the most appropriate resin (compatible with the required application), and suitable treatment of the surfaces. Indeed, each adhesive system has properties that are dependent on the specific characteristics of the adherend [15]. The success of adhesive bonding is commonly related to pre-bonding operations performed on the contact surfaces to obtain features such as good wettability, surface activation, increased chemical interactions between adherend and resin, and proper roughness extent for mechanical interlocking [16]. The most common methodologies for the pre-bonding preparation of plastic composites are based on purely mechanical actions on the surface morphology or roughness modifications that mainly promote mechanical interlocking, often at the expense of result repeatability along with contamination. Furthermore, despite abrasive techniques being easier to perform, they require more care in avoiding defects or delamination, which may strongly affect the joint strength. For this reason, in recent years, valid alternatives have been sought, and non-standard technologies have garnered increasingly widespread interest. In particular, plasma processes [17] provide advantages such as contaminant removal, surface activation, no need for hazardous chemicals, and ease in the processing management and automatization. Such features appear perfectly suitable to be combined with additively manufactured composite substrates, in order to obtain the maximum performance from adhesive joints. However, for its part, 3D printing must allow fabrication of composite components in such a way as to make any assembly operations possible, safe and reliable. Indeed, composite structures, and particularly those built additively, are inherently non-homogeneous. As stated by Iragi et al. [18], "under transverse and interlaminar loads (normal and shear) the mechanical response [of the composite] is strongly influenced by manufacturing defects […] such as a large number of voids, non-homogeneous distribution of fibres and poor bonding between beads and layers". This aspect was also discussed by Caminero et al. [19], who examined the interlaminar bonding performance of such materials, relating their behavior to process parameters such as layer thickness and fiber volume fraction.

Despite the joining of AM materials being a key area of study for manufacturing of structures of increased complexity [20,21], to the best of the authors' knowledge, the influence of the multilayer deposition on the characteristics of composite adhesive joints lacks references in the literature. Hence, this experimental work was focused on evaluating the mechanical and failure behavior of an adhesive system made of continuous-carbon-fiber (CCF) Nylon-6 composite substrates and epoxy adhesive, verifying how the AM substrates respond to adhesive bonding when the interface interactions are increased by preparing the surface with consolidated treatment methods for traditionally-manufactured CFRP materials. In particular, two main questions have driven the investigation: To what extent is it possible to obtain quality joints with 3D-printed composites? How does the inhomogeneity of the base material affect the joint behavior?

The experimental findings allowed the definition of the current performance threshold for the adoption of adhesive bonding to newly-printed composites. It was indeed demonstrated that, when the surface treatment creates adhesive-surface interactions that are stronger than those existing between the subsequent layers laid down to build the base material, the latter achieves its ultimate resistance, becoming the weak part of the adhesive system owing to its inherent discontinuity. Notably, this situation has been verified using low-pressure-plasma (LPP), which is confirmed to be effective for the treatment of the composite-adhesive interface.

The information obtained from the analyses has been considered pivotal to identify both the actual limitations of the manufacturing process affecting joint performance and promising approaches to overcome them. Therefore, this work is to be intended as a basis for future developments aimed at improving the joint characteristics by acting on substrate optimization.

2. Experimental details

2.1. Materials

The CFRT used as substrate material was additively manufactured using a Mark Two (Markforged® Inc., Watertown, MA, USA) FFF desktop 3D printer with a maximum build volume of 320 mm × 132 mm × 154 mm. As shown in Fig. 1, the printer is equipped with two separate extrusion nozzles, each dedicated to a different wire of raw material feed. Two types of filaments supplied by Markforged® were used to build the substrates: a Nylon-6 filament filled with chopped carbon fibers (traded as Onyx) which came in an initial diameter of 1.75 mm; and a filament made of continuous carbon fibers (CCF) embedded in a Nylon-6 matrix, having a diameter of 0.35 mm. The filaments were stored in a protective dry box to avoid ambient humidity absorption. The temperature of the printing heads for the Onyx and the CCF filaments was set to 265°C and 270°C, respectively, whereas the printing bed was non-heated.

The accompanying pre-processing and slicing Eiger® software was used to set printing parameters such as the fiber type, fill mode, fiber orientation, number of layers, and number of outer Onyx rings (Table 1).

The specimen geometry was created *via* computer aided design (CAD) software (SolidWorks 2016, Dassault Systems), exported as a

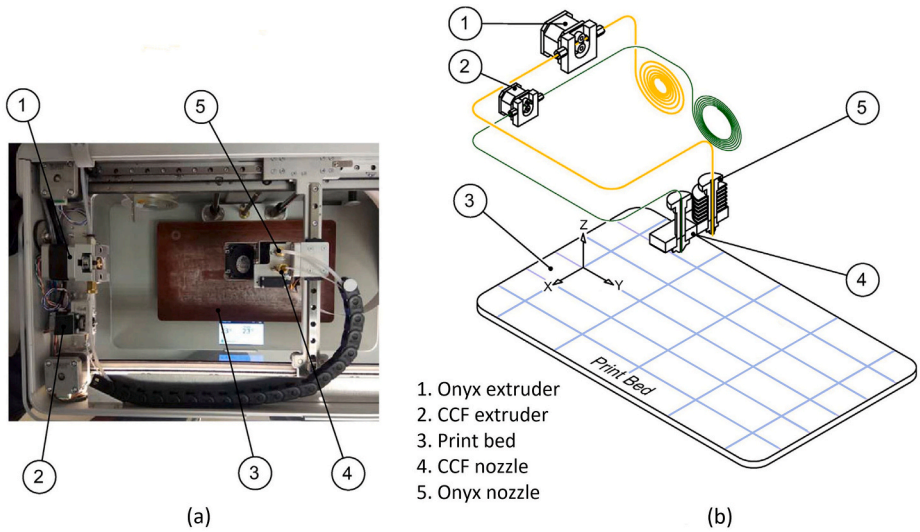

Fig. 1. Markforged® Mark Two FFF desktop 3D-printer. (a) General view and (b) scheme of the printing process (Adapted with permission from Ref. [19]).

Table 1
Main printing specifications.

Parameter	CCF	Onyx
Filament type	Continuous Carbon Fiber	Short-carbon-fiber reinforced PA6
Fill mode	Isotropic	Isotropic (infill) + Concentric (rings)
Fiber orientation	0°	±45°
Number of layers	8	8
Number of rings		2
Build orientation	Flat	
Layer thickness (mm)	$L_t^{CCF} = L_t^{Onyx} = 0.125$	

stereolithography file (STL), and imported into Eiger®, through which the material-laydown path was defined (Fig. 2). Each substrate was built with a 'flat' build mode on subsequent planes along the Z-direction (each parallel to the XY-plane of the printing bed) by stacking layers having CCFs with unidirectional 0°-orientation with respect to the axial dimension of the specimens (*i.e.*, along the direction of the load applied during mechanical testing), to maximize the performance of the substrate and, hence, of the joint. It is worth noting that Markforged® assigns the label 'Isotropic' to this fill mode, not referring to the mechanical properties of the final test specimen. In fact, an 'Isotropic' fill type determines creation of a test specimen having a unidirectional laydown of the continuous fibers, thus resulting in anisotropic behavior of the specimen. It should be also noted that Eiger® obliges the user to print every part by adding an outer protective shell made exclusively with Onyx (by means of layers arranged at angles +45° and −45° alternatively with respect to the axial direction), the extent of which is defined as a set-up parameter.

Therefore, each substrate was made of 16 layers (to obtain an overall sample thickness of 2 mm), comprising four floor layers made of Onyx, eight core CCF layers, and four roof layers chosen for dimensional accuracy and symmetry.[1] The final thickness of each layer was set to 0.125 mm for both Onyx and CCF. Onyx was also laid along the specimen perimeter to generate, layer by layer, two concentric rings. It follows that each substrate consisted of a CCF infill enclosed within a protective shell of Onyx only, as schematized in Fig. 2c.

[1] The number of roof/floor Onyx layers was set equal to four on the basis of preliminary print tests. It corresponded to the minimum value of shell layers that avoided premature detachment of the Onyx from the CCF support below.

The substrates were joined together by using the 3M™ DP490 adhesive, the technical characteristics of which are listed in Table 2. As described in Section 3.1, this adhesive was considered suitable for the current application, being designed for structural adhesive bonding requiring toughness and high mechanical strength, along with excellent thermal and environmental resistance. This two-component, thixotropic epoxy resin was prepared by mixing two parts of epoxy resin and one part of amine-modified curing agent. Complete crosslinking was obtained through 14-h curing at RT, followed by post-curing in an oven for one hour at 80°C, in accordance with the indications provided by the manufacturer.

2.2. Surface treatment and sample analysis

The surface treatments performed on the 3D-printed composite substrates are summarized in Table 3. Their different effectiveness was exploited to detect and highlight those criticalities that might limit the application of adhesive bonding to 3D-printed CCF composites.

To remove any trace of surface contaminants, a preliminary wiping with acetone was carried out on all the substrates to be joined. Two sets of samples, the bond areas of which were prepared with conventional methods, namely solvent degreasing and mechanical abrasion respectively, were used as references for the comparison. The abrasion was manually performed using a 3M™ Scotch-Brite™ MX-SR abrasive, repeating linear movements, at an angle of 45° between one pass and another. After this operation, the surfaces were once again wiped with an acetone-soaked cotton cloth, to remove all debris from the outer layer.

Low-pressure plasma (LPP) was instead selected because of its well-known effectiveness as prebonding treatment of polymer materials [14,15,22]. A Tucano multipurpose LPP reactor (Gambetti Vacuum Technology, Milan, Italy) was used to perform it. This device is powered by a radio frequency (RF) generator operating at 13.56 MHz, with a maximum power of 200 W. Through two Mass Flow Controllers (MFC), a certain percentage of process gas (as a single gas and mixtures of two gases) is introduced into the vacuum chamber. The latter contains the samples to be treated and is evacuated to a pressure level of 0.1 mbar. Then, the RF power supply is switched on to ignite the plasma discharge between the two electrodes. In this investigation, atmospheric air was used as the process gas, varying plasma power among the values listed in Table 3; an exposure time of 180 s was set, since this had already been found to be effective in LPP treatments on polyamide materials [23].

Before each measurement, all the specimens were dried for 1.5 h at 80°C; the analyses were then performed at controlled environmental

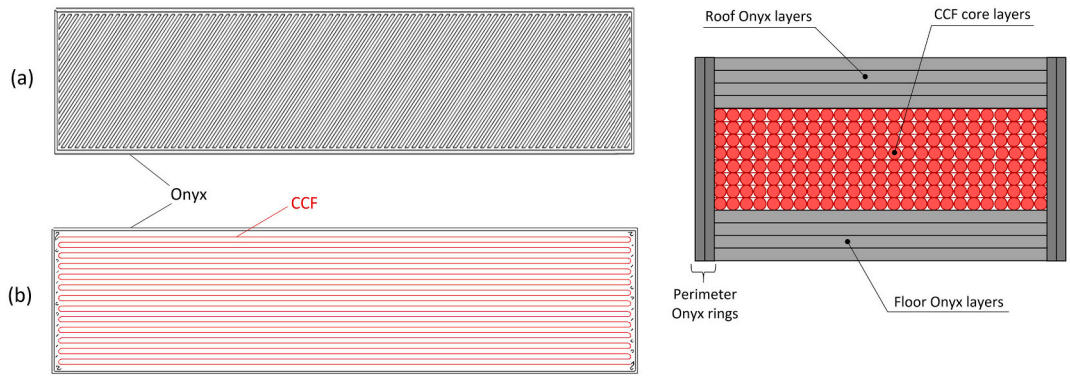

Fig. 2. (a) Laydown pattern of the outer Onyx-only layers and (b) unidirectional fiber pattern (0°) of a generic core-layer. (c) Schematic representation of the AM-CFRT substrate cross-section.

Table 2
Technical specifications of the 3M™ DP490 adhesive.

Characteristic	Base	Accelerator
Type	Epoxy	Amine-modified
Color	Black	White
Mix ratio	2	1
Work life	1.5 h @ 23°C	
Handling time	4 ÷ 6 h @ 23°C	
Curing conditions	14 h @ 23°C + 1 h @ 80°C	

Table 3
Surface treatments performed on the AM CFRT substrates.

Surface treatment	Description	
Degreasing	Acetone wiping	
Abrasion	Acetone wiping + 3M™ Scotch-Brite™ MX-SR + Acetone wiping	
LPP	Acetone wiping + Plasma treatment with the following set-up parameters:	
	Power (W)	50, 100, 150
	Exposure time (s)	180
	Gas	Air

conditions (T = 23±2°C, RH = 40±5%).

The morphological assessment was carried out using a Talyscan 150 (Taylor Hobson, Leicester, UK) non-contact laser profilometer. Surface portions were acquired, setting a scan speed of 4500 μm/s and steps spaced 5 μm apart. Data processing was carried out through the associated TalyMap 3D software, with which the roughness parameters were extracted from the areal acquisitions, in accordance with ISO 25178 [24]. Among them, root mean square (RMS) roughness, S_q, was selected to be provided as a result, it being more sensitive to large deviations from the mean line.

The same instrument and settings were also used to acquire the fracture profiles for the failure mechanism evaluation. A Zeta20 3D (Zeta Instruments, San Jose, CA, USA) optical, confocal profilometer was also used to inspect the sample surfaces and for further measurements aimed at acquiring more information about failure mechanisms.

The wettability of the surfaces was evaluated through measurements of apparent contact angle (CA) of deionized water. The assessment was performed with an OCA 20 (DataPhysics Instruments GmbH, Filderstradt, Germany) optical tensiometer, working in sessile-drop mode. The water-drop volume was kept constant and equal to 6 μL, and ten droplets were deposited on each substrate. For each droplet, the CA was determined as the mean between the two values acquired at the right and left sides of the drop profile. The relative images were captured and then digitized using the instrument software, SCA 20.

X-ray Photoelectron Spectroscopy (XPS) analyses were performed using an Axis Ultra^{DLD} spectrometer (Kratos, Manchester, UK) to assess the chemical state of the differently treated surfaces. The instrument was fitted with a monochromatic Al Kα source (photon energy = 1486.6 eV) operating at 15 kV and 20 mA, and areas of 300 μm × 700 μm were analyzed. High-resolution scans were carried out at a pass-energy of 10 eV and steps of 0.1 eV. Data acquisition was performed in ultra high-vacuum conditions, at a base pressure of the analysis chamber below 6×10^{-9} mbar. Charge calibration of the spectra was undertaken with respect to the main line of the C 1s spectrum (C–C bonds), the binding energy of which was set to a value of 285 eV. The CasaXPS software (version 2.3.18) was used for peak deconvolution and data fitting; Shirley-type background and Gauss-Lorentz profiles were adopted.

2.3. Adhesive-joint manufacturing and mechanical testing

Shear testing was performed to assess the mechanical response of the adhesively-bonded CFRT-to-CFRT joints. The composite substrates were built additively, following the printing criteria described in Section 2.1, in accordance with the geometries suggested by ASTM D1002 [25] for the manufacturing of single-lap joints (SLJ, Fig. 3). Five specimens (N=5) per set of treatment conditions were made and then tested to failure, allowing obtainment of the mean values to be provided in the Results section together with the related values of standard deviation.

In every case, both the adhesive bonding and all surface characterizations were performed within 15 min of treatment to prevent any further modification of the surface or deterioration of the treatment effect. The 3M™ DP490 adhesive was applied to the bond area of both substrates to be joined, and the latter were placed in contact with a 12.5 mm overlap along the major axis. A sheet of non-stick paper of calibrated thickness was used to control the adhesive thickness, which was fixed at 0.25 mm. Any excess resin was squeezed out from the interface by pressing the joint and then removed. Fixing tables were used to keep the joint in position throughout the adhesive curing time, guaranteeing perfect alignment of the two laminates.

An Instron 8802 Universal Testing machine (Instron, Norwood, MA, USA), equipped with a 50 kN load cell, was used to perform tensile shear strength (TSS) testing, for which a crosshead displacement rate of 1.3 mm/min was set. In Fig. 4, a scheme of the SLJ loading condition is illustrated, and a photograph of a real specimen installed on the testing machine is also provided.

As a result, the shear strength τ was calculated as:

$$\tau = \frac{F}{A_0} \tag{1}$$

where F is the ultimate load at failure and A_0 is the initial overlap area, equal to 25 mm × 12.5 mm.

During TSS testing, the alignment of the bond area along the centerline between the grip faces was ensured by placing shims, having

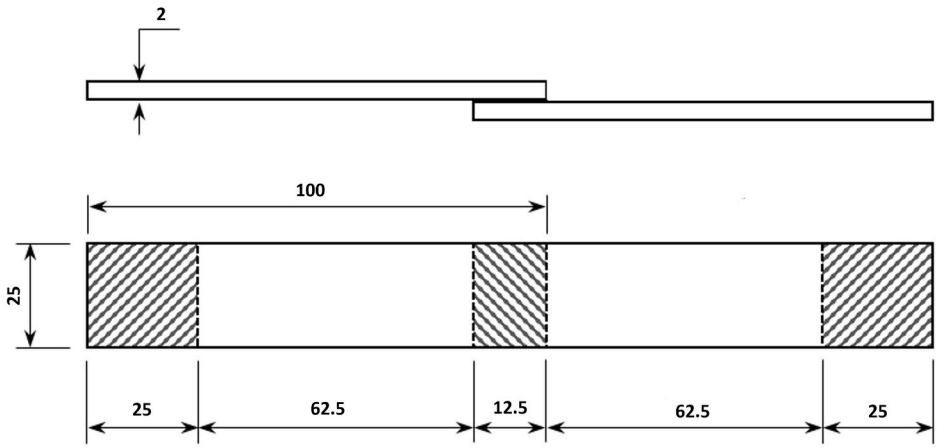

Fig. 3. SLJ geometry, according to ASTM D1002 (values in mm).

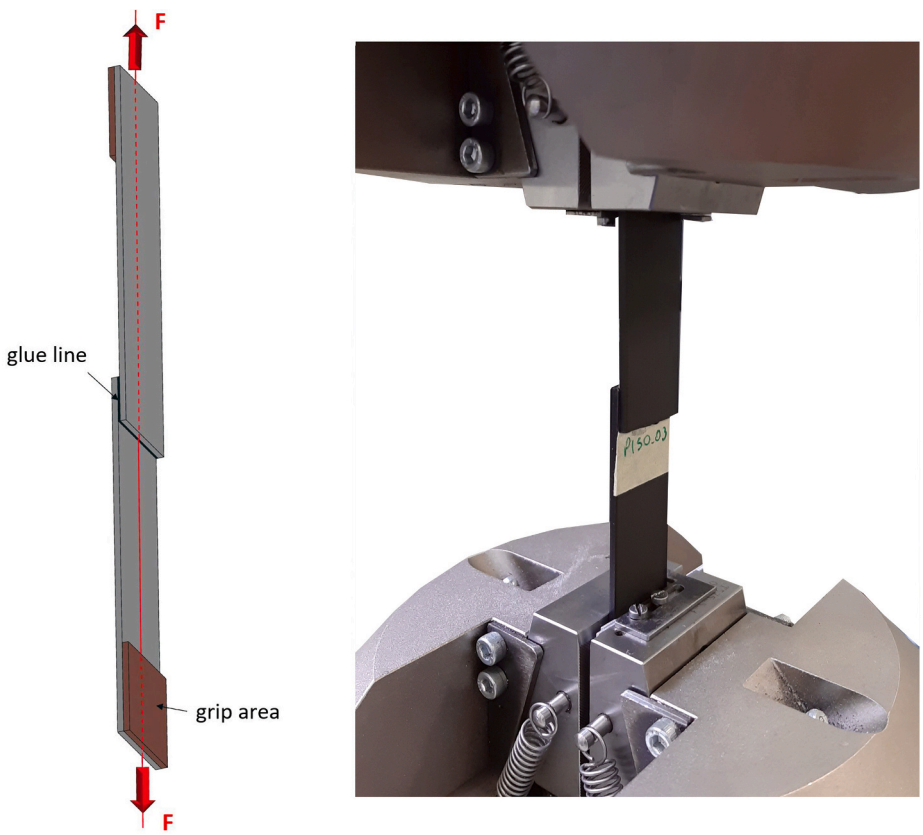

Fig. 4. Testing scheme for the TSS evaluation and real specimen installed on the machine before testing.

dimensions 25 mm × 25 mm × 2 mm, at the grip areas. Tests were performed at environmental conditions of T = 23±2°C, RH = 40±5%.

3. Results and discussion

3.1. Preliminary characterization of the base material

Performance of the base material and severity of the applicative scenarios should drive process engineers in the choice of adhesives and pre-bonding treatments that allow fabrication of joints able to satisfy quality requirements in line with those of the overall structure. For this reason, the determination of maximum strength achievable by the additively-manufactured composite was considered fundamental to set a preliminary benchmark, based on which to design the adhesive system.

Tensile testing was performed following the specifications summarized in Table 4. In particular, five tensile specimens of dimensions 157 mm × 16 mm × 3 mm were built according to the ASTM D3039 standard [26], following the same construction criteria used to create the joint substrates: a layer thickness equal to 0.125 mm was set to laydown both the Onyx and the CCFs, for a total of 24 layers. These specimens were then tested to failure using the Instron 8802 testing machine, setting a crosshead displacement rate of 2 mm/min.

As a result, the stress-strain curves displayed in Fig. 5 were obtained. It should be mentioned that these curves are those obtained from the displacement of the crosshead and used to obtain the strength parameter. An extensometer was instead used during the initial stage of the test to obtain the stiffness parameter (*i.e.*, elastic modulus *E*).

The 0°-CCF laydown pattern led to high resistance and stiffness of the

Table 4
Testing specifications and tensile properties of the base material.

Method	Test standard	Sample dimensions (mm)	Onyx layers	CCF layers	Maximum tensile strength, σ (MPa)	Elastic modulus, E (GPa)
Tensile	ASTM D3039	157 × 16 × 3	8	16	566.1 ± 13.6	24.2 ± 0.2

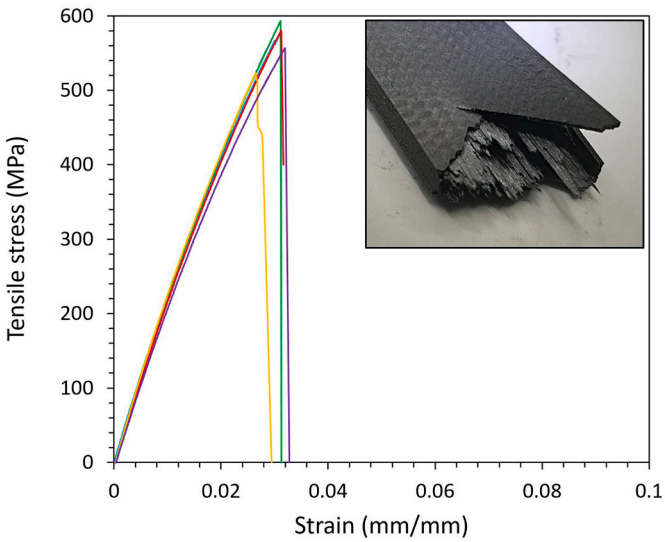

Fig. 5. Stress-strain curves acquired from tensile testing on the base material and related failure mode.

base material, which achieved average tensile strength of about 566 MPa, in line with the values found in the literature focused on similar laydown configurations [12]. Failure occurred due to the sharp fiber breakage in the specimen core. After complete rupture, a slight detachment of the roof/floor Onyx shell from the CCF core below was also observed, as shown in the inset of Fig. 5.

As mentioned above, the adhesive selection was carried out sizing the potential joint performance on the base-material strength. As stated by Mandolfino and co-workers [23,27], good response to LPP treatment of injection-molded polyamide-6 substrates is, in principle, achievable by using acrylic adhesives. However, since epoxy adhesives are generally more suitable to face the typical severity of the applications involving reinforced plastics [28], a resin of this kind was used in the study. Specifically, 3M™ DP490 adhesive was selected to correlate the behavior of the 3D-printed SLJs to that of joints made of traditional epoxy-matrix CFRP bonded through the same resin, reported in the literature [14,15].

3.2. Post-treatment surface state: morphology and chemistry

More information about the after-treatment surface state was considered necessary firstly to allow correlation between the mechanical behavior of the SLJs and the phenomena involved in the treatments of the Onyx shell. Secondly, this assessment was also essential to exclude the presence of any damages of the substrate as a result of the treatments adopted. Hence, surface analyses were preliminarily performed on substrates that simulated the same conditions as before the adhesive application, specifically, degreased-only (indicative of the as-received surface condition), abraded, and LPP-treated surfaces. Concerning the latter, on the basis of the mechanical findings and the relative fracture behavior discussed in Section 3.3, only the surface appraisals relative to the 50-W LPP case will be presented.

A first analysis focused on the detection of any macroscale morphological modifications generated on the surfaces. Given the large size of the surface features in both XY-plane and Z-direction, a further analysis with optical confocal profilometer was carried out to inspect areal portions at higher magnification (20×) for microscale roughness evaluations. In this regard, refer to Fig. 6, which shows 3D topological maps acquired *via* laser profilometry on the three different treated surfaces and related high-magnification images. The as-received surface (*i.e.*, degreased-only) presented a mean RMS value (S_q) of 13.9 μm. The sample exhibited the typical 45°-pattern arrangement used to print the outer Onyx layer, also showing short carbon fibers aligned along the extrusion direction (Fig. 6a). In contrast, an in-depth morphological modification was obtained with abrasion (Fig. 6b): compared to the former, the aforementioned infill pattern was made smoother and, hence, it was no longer identifiable (S_q was 7.0 μm on average). However, higher magnification (20×) made it possible to detect narrow grooves generated by the mechanical action of the abrasive on the sample surface. No significant variations from the as-received sample were instead observed after plasma treatment (Fig. 6c), the latter having left the surface macroscopically unchanged both in terms of topological structure and roughness parameter values (S_q = 13.8 μm). Such observations also found confirmation in the microscale measurements, which emphasized the similarity of the two cases, both characterized by profiles having large peak-peak step-heights (typically, larger than 20–30 μm). Nevertheless, this situation does not exclude that physical LPP treatment may have changed the Nylon-6 surface on a lower roughness scale. In principle, this might even have significant influence on the bonding mechanism at the molecular-scale, where secondary valence bonds (e.g., van der Waals forces) can contribute to the interactions between material and resin [29].

A topological evaluation should be combined with the analysis of the wettability of the surface, since the non-wetting condition may prevent adhesive bonds from forming at all. Therefore, wetting properties of the samples were determined by depositing droplets of deionized water on each surface and measuring apparent CA wherever possible. To emphasize the different behavior exhibited by the three surfaces after treatment, in Fig. 7 the values of drop diameter over time acquired immediately after deposition are displayed; in the insets, the shape assumed by the droplet is also provided. CA of the degreased sample (Fig. 7a) was 83.9° on average, whereas the abraded surfaces (Fig. 7b) exhibited hydrophobic behavior, with CA of 100.0°. The difference between the two cases has to be associated with the relationship between roughness and air trapped in the surface asperities, as suggested by the Cassie-Baxter wetting model [30]. As previously mentioned, the effect of abrasion on the macroscale morphology is that of smoothing of the surface pattern with respect to the as-received sample. However, at the micro-scale, abrasion yields narrow, deep grooves into which the droplet might not be able to penetrate. It follows that the drop results, to a certain extent, deposited on air trapped in grooves. This condition determines higher values of CA, hence, suggesting more hydrophobic behavior of the surface. Despite their different behavior, in both cases, the droplet achieved a stable diameter a few seconds after deposition. In contrast, a sharp transition from spherical to flattened droplet shape was observed after plasma treatment. Indeed, the surface of the LPP-treated sample exhibited super-hydrophilic behavior. Consequently, in this case, measuring CA was not possible since each droplet deposited resulted completely spread on the sample surface (Fig. 7c), not allowing correct data acquisition (the fluctuations in drop diameter are due to the software's inability to distinguish the droplet profile from the surface). The perfect wettability of the so-treated sample has to be related to the oxidizing effect of plasma, which stimulates an increase of polar species on the Onyx surface, developing its hydrophilicity.

Indeed – as detected *via* XPS analysis by comparing the three

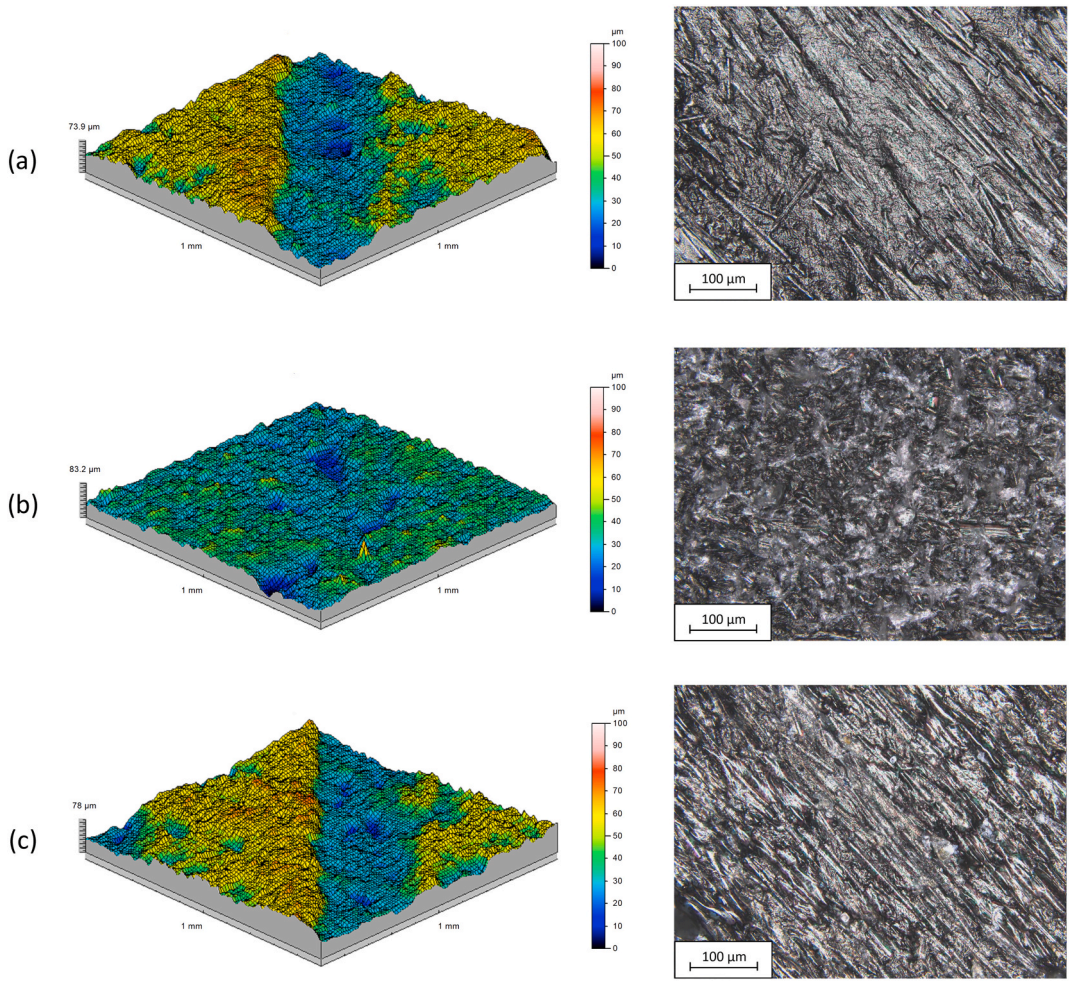

Fig. 6. 3D Morphological maps (left) and 20×-magnified images (right) of AM-CFRT after (a) solvent degreasing, (b) mechanical abrasion, or (c) 50-W LPP treatment.

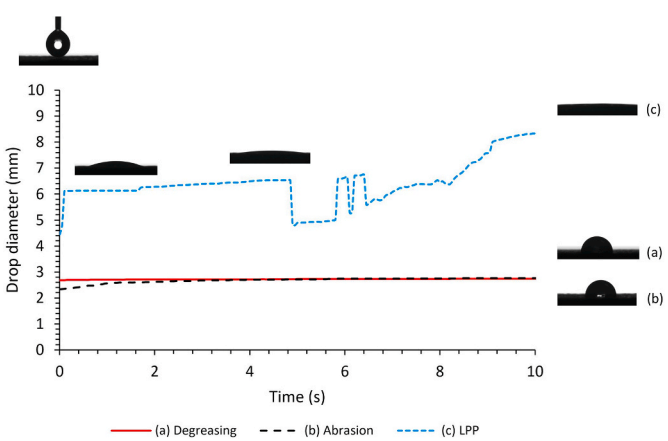

Fig. 7. Drop-diameter trend over the acquisition time relative to (a) degreased, (b) abraded, and (c) LPP-treated samples. The profiles assumed by the droplets after deposition are provided in the insets.

conditions of the Onyx surface after treatment (Table 5) – plasma treatment determined an increase in oxygen content together with a decrease of the carbon one, *i.e.*, an oxidative effect that was reflected in a significant increase of the oxygen/carbon ratio (+133%) with respect to the degreased-only CFRT surface, which can be taken as a reference. No significant changes at the N 1s peak were observed instead, and thus the increase in the N/C ratio is only due to a decrease of C 1s.

Table 5
Atomic percentages of oxygen, carbon, and nitrogen, and related O/C and N/C ratios, obtained through XPS analysis.

Surface treatment	Atomic percentage (%)				
	O 1s	C 1s	N 1s	O/C ratio	N/C ratio
Degreasing	26.0	67.9	6.1	38.3	9.0
Abrasion	23.5	70.1	6.4	33.5	9.1
LPP	44.1	49.8	6.1	88.6	12.2

To focus on the specific effect of the LPP treatment on oxidation and activation of the Onyx surface, high-resolution XPS investigation was performed on the energy regions located around the C 1s (282 ÷ 292 eV) and the O 1s (528 ÷ 540 eV) peaks. The results of these analyses are reported in Fig. 8; they demonstrate that the LPP treatment had a significant effect on the shape of both the carbon and the oxygen peaks. On the other hand, spectra collected on degreased-only and mechanically abraded surfaces do not differ significantly one from the other.

The positions (*i.e.*, binding energy, BE) of the peaks detected after deconvolution of C 1s and O 1s peaks are in good agreement with those expected from a generic pure-Nylon-6 reference surface [31]. However, it should be noted that the Onyx surface differed from the XPS spectra of Nylon-6 reference in terms of intensity of C 1s main peak, which was higher for the Onyx owing to the presence of the short carbon fibers exposed on its surface (also visible in Fig. 6). Notably, deconvolution of

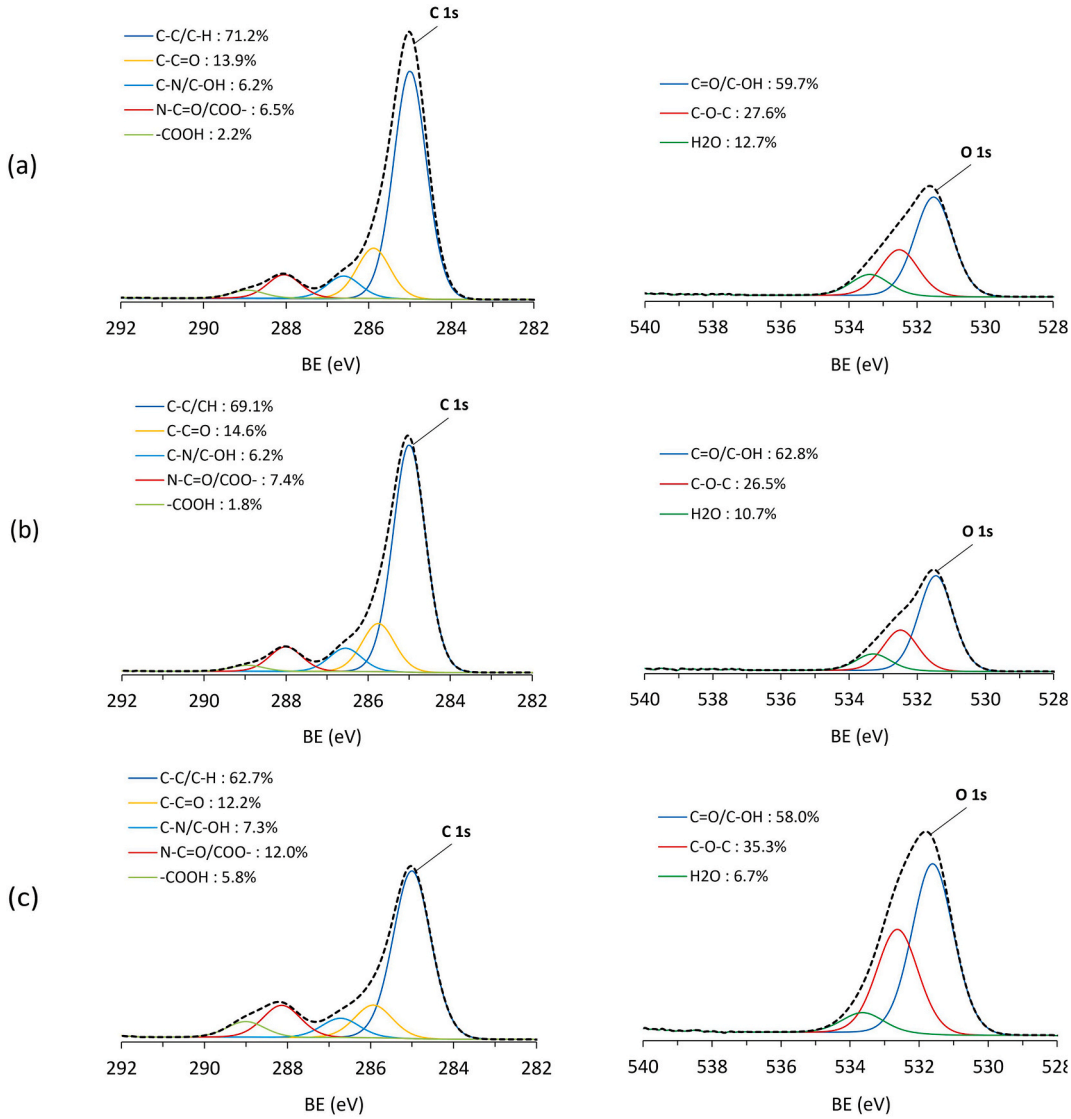

Fig. 8. High-resolution XPS spectra representing the C 1s (on the left) and the O 1s (on the right) peaks acquired on the AM-CFRT surfaces after the following preparations: (a) solvent degreasing, (b) mechanical abrasion, (c) 50-W LPP. In the key, each chemical species detected is quantified in terms of area percentage.

the C 1s peak allowed identification of various carbon components related to: single bond between carbon and carbon or carbon and hydrogen (C–C, C–H) positioned at 285.0 eV, carbon singly bound to a C═O bond at 285.7 eV, or to nitrogen (C–N) at 286.6 eV. A typical peak of the Nylon-6 corresponding to carbon forming a single bond with nitrogen and a double bond with oxygen (N–C═O) was recognized at 288.0 eV, while a further carboxyl group (COOH) was found at 289.0 eV. The parallel deconvolution of the O 1s spectrum highlighting the presence of two different chemical species: the first, at about 531.5 eV, was interpreted as oxygen making a double bond with carbon (C═O) or carbon forming a single bond with hydroxyl (-OH). The second, positioned at 532.5 eV, corresponded to a C–O–C group.

From a comparison between the pre- and post-treatment conditions, the decreasing trend of carbon-hydrogen bonds is reasonably intended as a direct effect of the increasing oxidative reactions produced by plasma treatment, which involved the generation of bonds between oxygen and carbon atoms. Hence, LPP of the surfaces created free radicals able to couple with the active species present in the plasma environment, leading to reactions that are essential for the changes in the surface functionalities. The introduction of newly formed functional/additional groups, along with the possible presence of low-molecular weight oxidized materials (LWMOM, consisting of oxidized short polymer fragments, such as monomers or oligomers) [29], led to an enhancement of the surface polarity, entailing the hydrophilic behavior of the Onyx surface.

3.3. *Joint performance and failure mechanism*

Knowledge of the limits achievable by the multilayer system is particularly important considering that, for many applications, assembly *via* adhesive bonding is an integral part of the manufacturing process. Of course, the distinctive advantages of composite substrates also have to be guaranteed by their joining. As the previous mechanical characterization of the base material showed, the 3D-printed composite has the potential for manufacturing components having strength and stiffness comparable to those of more traditional CFRP. This result, in principle, would make plasma one of the most suitable methods to prepare the composite surfaces and obtain quality joints. Indeed, the experimental findings reported in Section 3.2 confirmed that, also for the Onyx surface, plasma treatment is effective in creating interface conditions that are appropriate to adhesive bonding. Despite this, the application of a high-performing treatment on the 3D-printed composite substrates may be thwarted owing to the intrinsic non-homogeneity of the base material, as discussed in the following.

The different effectiveness of the surface treatments examined was exploited to detect and highlight the system criticalities. In this regard, Fig. 9 shows the load-displacement curves recorded testing the composite SLJs, whereas in Table 6 the test results are listed, together with indications of the related failure modes observed.

Generally speaking, mechanical tests confirmed a remarkable increase in shear strength of the adhesive-bonded SLJs due to plasma treatment compared to traditional pre-bonding methods, such as simple degreasing (Fig. 9a) or mechanical abrasion (Fig. 9b). TSS of the degreased-only joints was 4.5±0.3 MPa, whereas after mechanical abrasion of the faying surfaces, its value was about 29% more (5.8±0.3 MPa). To explain the enhanced joint resistance observed after abrasion with respect to the former, a consideration has to be made about the viscosity of the adhesive used. Indeed, speed and depth of the adhesive infiltration within the surface irregularities depend on the rheology of the adhesive itself, just as it is in this case, where the viscosity of 3M™ DP490 epoxy adhesive may reduce its penetration ability. Consequently, a reduction in macro-scale roughness led to improved shear performance since the actual contact area increased. However, in both cases, failure was 100% de-adhesive in type (AF) since it always occurred at the interface between resin and substrate, thus proving weak adhesion interactions between the two. Indeed, after joint failure, one of the two contact areas appeared smooth as the adhesive layer (0.25 mm in thickness) remained firmly attached to the other surface, as also detectable from the fracture profiles shown in Fig. 10a and b.

Contrariwise, the LPP treatment determined a significant improvement in the mechanical behavior of the joints, with an increase in shear strength up to 224% more than that of the abraded joints. Such a result can be explained as the effect of the chemical state modification due to LPP. In particular, the increased number of polar groups supplied more reactive sites for interfacial bonding between the Onyx layer at the surface of the CFRT material and the epoxy adhesive applied, thus leading to better mechanical performance of the joints.

As described in Section 2.2, LPP treatment was performed using three power levels (50, 100 and 150 W) in an attempt to make any variations in mechanical or failure behavior evident. Indeed, the preliminary XPS analysis suggested that LPP treatment leads to increased oxidation of the chemical species present on the sample surface. As discussed by Štepánová et al. [32], oxidation of polymer surfaces may achieve a threshold level by increasing the treatment energy (defined as the relationship between input power and exposure time). In this condition, production of low-molecular-weight materials can take place as a consequence of surface chains' scission, with ensuing formation of LMWOM that may affect adhesion negatively. Nevertheless, the three differently-powered plasmas uniformly led to substrate failures (SF), making it impossible to distinguish the relative chemical effect on the joint performance. Indeed, although the deviation between the results appeared quite large, this aspect was attributable to the heterogeneity of the substrates rather than to different interfacial conditions.

Table 6
Results of shear strength measurements for the different treatment conditions.

Surface treatment				Maximum load (N)	TSS (MPa)	Failure mode
Degreasing				1395 ± 87	4.5 ± 0.3	Adhesive
Abrasion				1812 ± 82	5.8 ± 0.3	Adhesive
LPP	Gas	t (s)	P (W)			
			50	5873 ± 134	18.8 ± 0.4	Substrate
	Air	180	100	5275 ± 357	16.9 ± 1.1	Substrate
			150	4633 ± 306	14.8 ± 1.0	Substrate

Overall, shear testing of the SLJs highlighted two aspects of main interest, summarized as follows:

- with this adhesive system, mechanical abrasion alone cannot be considered as a valid pre-bonding solution to obtain quality joints, since the increase in shear strength relative to simple degreasing of the surfaces would not be enough in most of the applications in which composite materials are used. It follows that more effective treatments are needed to reach proper quality for the adhesive-bonded assemblies, making their performance adequate to that of the rest of the structure built in CCF-reinforced plastic. In principle,

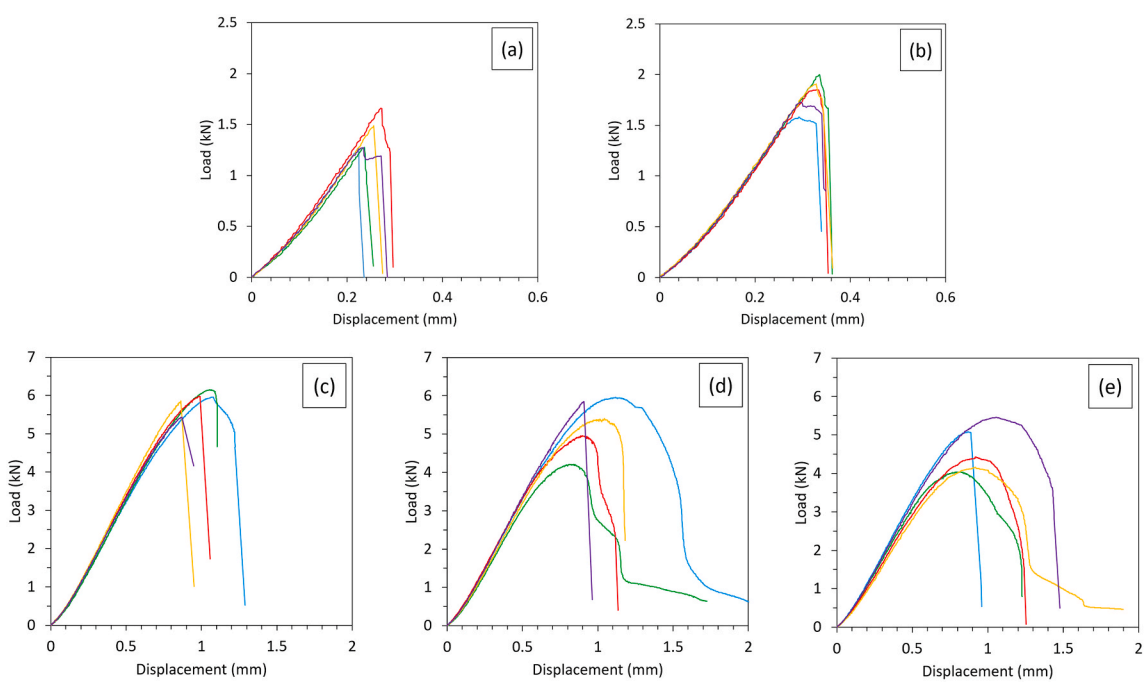

Fig. 9. Load-displacement curves obtained from TSS testing of SLJs adhesively bonded after the following preparations: (a) solvent degreasing, (b) mechanical abrasion, or low-pressure plasma at (c) 50 W, (d) 100 W, (e) 150 W. To draw each graph, five specimens per set of surface conditions were tested, and the curve referred to each repetition is displayed.

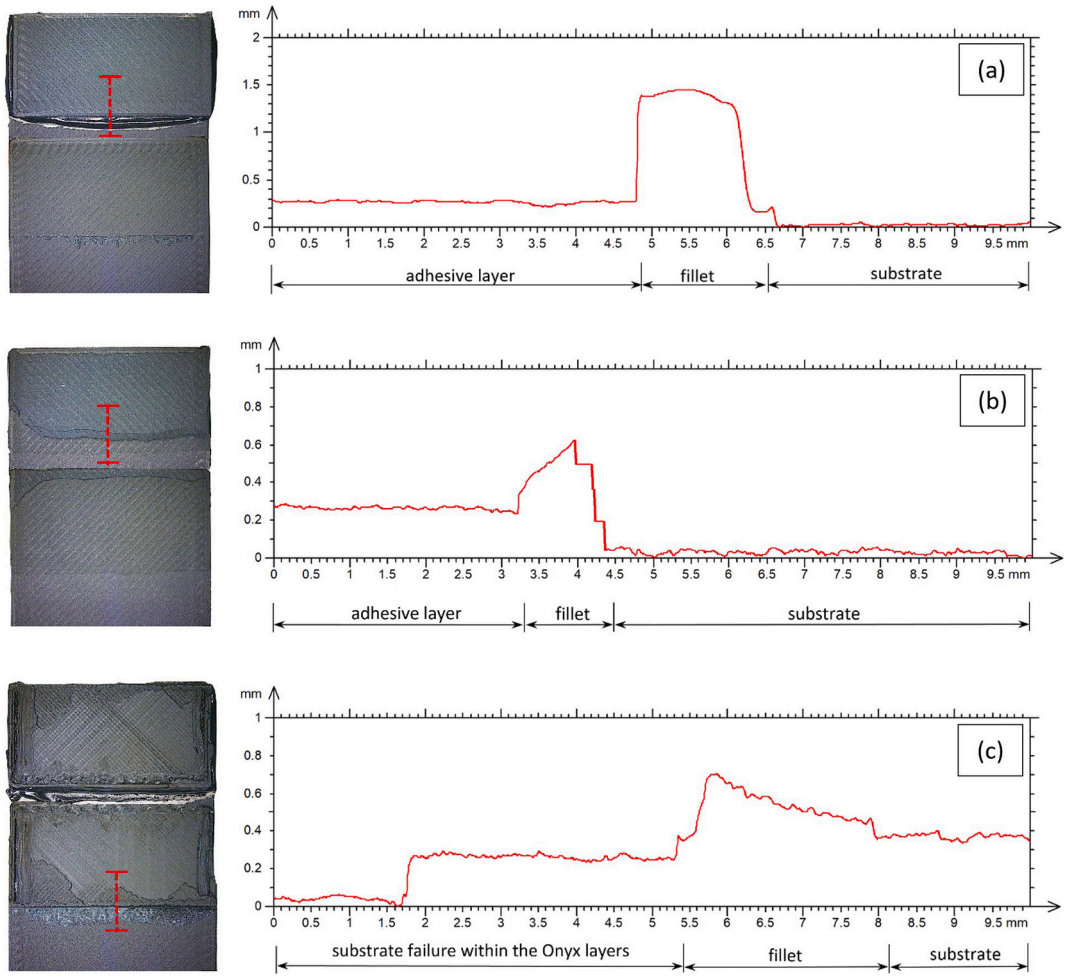

Fig. 10. Fracture areas and related failure profiles of (a) degreased-only, (b) mechanically abraded or (c) LPP-treated SLJs, acquired along the corresponding dotted lines.

LPP is a preferable choice to treat the Onyx surface as it leads to interfacial conditions that make the adhesive interactions between substrate and resin strong and stable;

- the stronger the adhesion forces at the adhesive-Onyx interface were, the more vulnerable the base material proved to be, the latter becoming the weakest part of the overall adhesive system. Indeed, as observable from the load-displacement curves related to LPP-treated SLJs (Fig. 9c–e), before reaching the ultimate load, a progressive reduction of the curve slope took place. This non-linear region has to be associated with plastic deformation and fracture propagation within the matrix of the composite. Despite the substrates having been built with the same conditions and having failed similarly, a lack of repeatability was observed among the results, making each rupture unpredictable.

Focusing on the latter point, the identification of the joint failure mechanism was deemed fundamental to supply further information/data that might guide the additive criteria for composite printing. Indeed, as discussed earlier, the multilayer substrate did not prove its limits until a high-performing treatment was employed. In this case, failure profile measurements demonstrated that the cracks always propagated within the substrate following specific planes, which corresponded to certain built layers. In particular, two locations appeared to be weak points for the substrate: the Onyx-to-Onyx interface, where

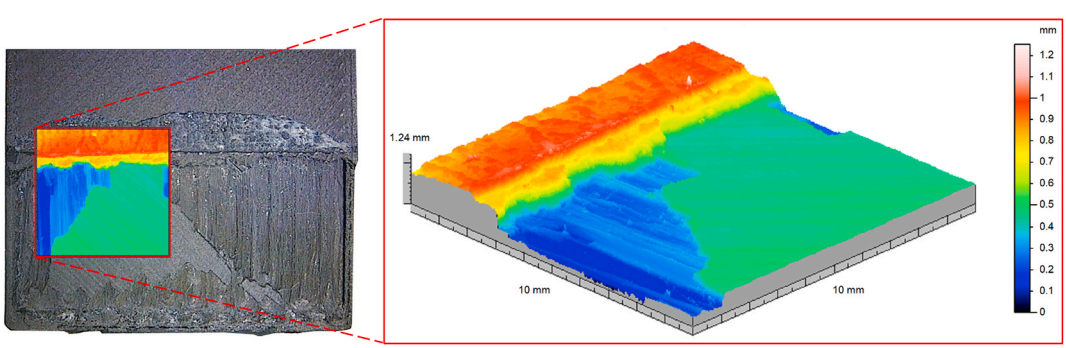

Fig. 11. Fracture area of an LPP-treated SLJ. Crack propagated both within the Onyx outer shell and at the Onyx–CCF interface.

detachments between subsequent layers composing the outer shell of the specimen occurred (Fig. 10c); and the interface between the Onyx shell and the CCF layer just below (Fig. 11).

Owing to the failure location, such behavior is considered strictly related to the failure mode observed from the tensile testing performed on the base material, where a detachment of the Onyx shell from the CCF core below was detected, suggesting poor adhesion between them. This condition is presumably due to concurrent effects related to the interlaminar bonding performance of the base material, and the mechanics of the SLJ stressed to shear.

Examination of the substrate cross-section at different magnifications (Fig. 12) confirmed that the overall size of both the Onyx roof and CCF core differed from the values expected. Indeed, it should be remembered that each layer should have a thickness of 125 μm, the latter being defined as a set-up parameter of printing. Nevertheless, an extra size of 79 μm was detected on the Onyx side (+15.8% with respect to that expected), whereas the extent of the CCF core exceeded the reference of 77 μm (+7.7%). Moreover, higher-magnification acquisition allowed detection of a detrimental, small gap (approximately equal to 19 μm) at the interface between Onyx and CCF. These observations are perfectly coherent with the two failure modes exhibited by the SLJs tested for shear, and find a reasonable explanation in the literature. Indeed, as Caminero et al. [19] stated, maximum achievable strength in 3D-printed CCF composites is limited by both the matrix-matrix and fiber-matrix interactions in portions that may be rich in porosities and voids. The latter are intrinsically due to the printing procedure, in which neither pressure nor external heating is applied after the layer is laid down. As van de Werken et al. [33] observed, the out-of-oven, layer--by-layer fabrication procedure typical of FFF is affected by the cooling of the deposited layer below its glass transition temperature before the following layer is deposited, therefore limiting interlayer bonding. The absence of a further consolidation step leads to interlayer defects, typically resulting in material discontinuities (e.g., triangular or quadrangular voids) – the number and extent of which are not easily predictable – that might act as sites of stress concentration and crack initiation. This aspect has been reflected in different load-displacement trends exhibited by the three LPP-treated sets of joints, which are related to interlaminar bonding phenomena affecting base material, independently of the parametrizations adopted for plasma treatment.

The under-load behavior and failure mode of the plasma-treated joints were further emphasized by the mechanics of TSS test, to which the higher ductility of the Onyx (in direct contact with the adhesive) relative to the stiffer CCF-core also contributed. Indeed, during shear testing, the load is applied aligned to the centerline of the SLJ, but – depending on the substrate stiffness - it might also produce a slight bending moment that progressively makes the joint section rotate. In principle, the rigid adherend core, designed of multiple CCF layers, contrasts bending, minimizing its value. Nevertheless, the system is not homogeneous, and thus neither is its response. Indeed, based on the nature of the outer shell, greater deformations occur on the Onyx side. As previously discussed, the outer Onyx layer shows increased bonding capacity towards the adhesive after LPP treatments. Such a condition makes the Onyx shell become an intermediate, ductile layer between the epoxy adhesive and the substrate core, thus having completely different mechanical properties from the latter. As schematized in Fig. 13, during TSS testing, such a multilayer configuration of the joint makes the Onyx slip on the CCF core below, progressively causing interlaminar failure within the bulk and/or peeling from the composite support.

This behavior has a severe impact on the joint integrity and thwarts any effort made to optimize the system in making it robust in terms of adhesive selection and surface treatment. Indeed, both weakness of interface bonds between contiguous layers and material discontinuities are, at this stage, practical issues that may strongly limit the use of adhesive bonding for those applications in which traditional polymer composites are commonly joined through resins. This aspect is all the more evident when comparing the performance of the AM-CFRT joints to that of joints made bonding CFRP parts fabricated through traditional methods. In this regard, the results published in two works by Pizzorni et al. [14,15] can be taken as references for the current study, thanks to similar conditions of both adhesive (3M^{TM} DP490) and surface treatments involved. Precisely, in Ref. [15], after an extensive testing campaign on carbon-fiber-reinforced-epoxy SLJs, it was found that an

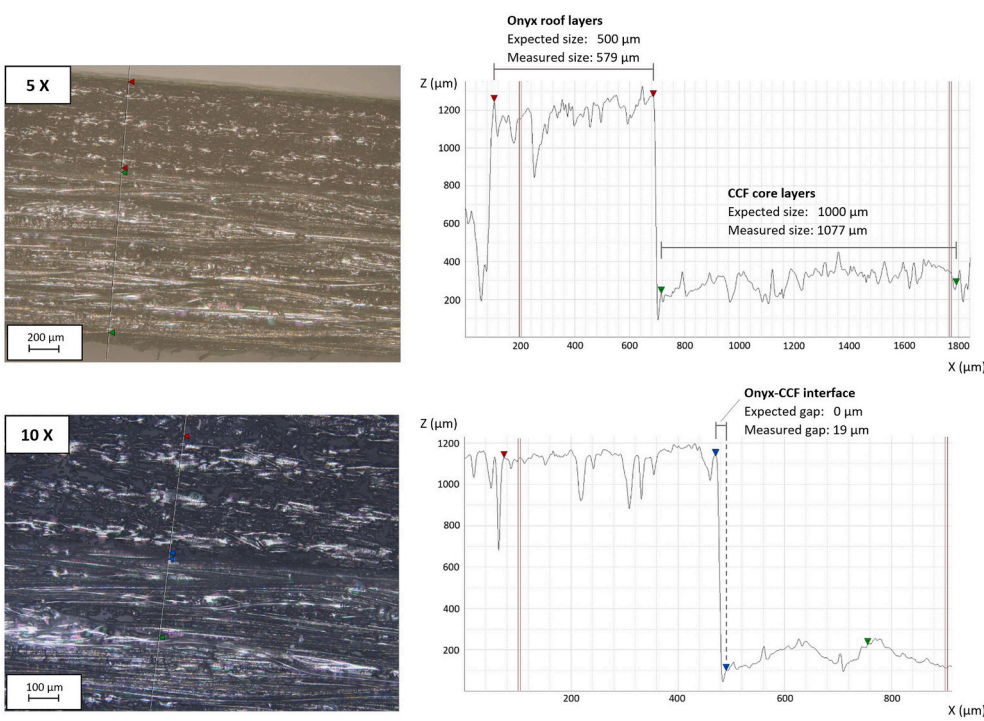

Fig. 12. Cross-sectional view of the 3D-printed substrate at different magnifications (5×, above, and 10×, below), and related measurement of the real extent of Onyx roof and CCF core compared to the expected values based on the printing settings.

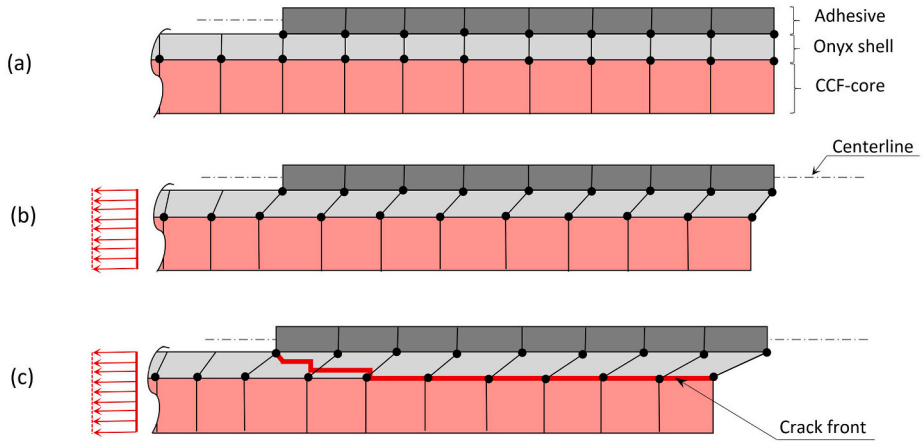

Fig. 13. Schematization of the mechanism of crack propagation at the Onyx-CCF interface during TSS testing of joints in high-performing conditions of treatment: (a) unloaded configuration, (b) under-load deformation and (c) subsequent slip of the Onyx layer on the CCF support, with crack propagation.

optimized air-LPP treatment enhanced shear strength up to 44.7% (27.3 MPa) with respect to conventional preparations. The characteristics of improved CFRP SLJs were further investigated in Ref. [14], resulting in shear strength of 31.2 MPa after air-LPP treatment, together with increased joint durability under hygrothermal aging conditions. In both cases, rupture of the plasma-treated joints was always cohesive in type, leaving the substrate intact after testing. Considering such behavior as a benchmark for composite joints, it is clear that the newly-printed joints are still far from this target. Nevertheless, these limitations might be reduced by implementing the AM process with post-printing phases, specifically, considering post-compacting processes as those applied to traditionally-manufactured (prepreg, infusion, etc.) CFRP. In this regard, a recent work by Mei et al. [6] focused on the further hot press of PA6-CCF composites having hybrid configurations similar to that of the current work. In their study, the authors investigated the tensile behavior of base material processed by varying post-process conditions of temperature, pressure, and time, demonstrating improved quality of the fiber-matrix interfacial bonding and, hence, better consolidation of the composite. Therefore, based on such results, it is reasonable to consider that post-printing compaction of the laminate through hot-press or autoclave cycles is likely a promising method to promote both interlaminar bonding and reduction of air gaps induced during substrate fabrication.

Another aspect worth considering is related to the evaluation of the adhesive-substrate combination. As mentioned earlier, the potential structural application of 3D-printed composites, in principle, would require the adoption of structural resins like the epoxy used here. However, it cannot be excluded that an improvement might be obtained reducing the adhesive stiffness. One possibility is the use of more ductile, structural resins (e.g., hybrid epoxy-polyurethanes) that might be exploited to reduce stress concentrations at the edges of the bond area. Alternatively, adhesive tailoring methods are studied today to control the elastic modulus along the bond line [20], e.g., increasing stiffness at the center of the joint, and progressively reducing it proceeding to the ends (*i.e.*, modulus tailoring), providing hybrid characteristics to the adhesive, as suggested by Kumar et al. [34].

Such possible approaches and related process strategies are currently subject of further investigation by the authors.

4. Conclusions

Additively-manufactured composite components are increasingly being used to create structures that are larger than the print build-volume of desktop 3D printers. For this reason, the relative design criteria are typically based on building-block approaches, leading to a manufacturing process of which assembly *via* adhesive bonding is an integral part. Therefore, in this research, the mechanical and failure behavior was investigated of an adhesive system made of mixed Onyx-CCF composite substrates additively manufactured *via* FFF and epoxy adhesive. A comprehensive experimental campaign was carried out to define how such a system responds to adhesive bonding after different surface treatments, using conventional pre-bonding preparations (degreasing or abrasion) and a more effective low-pressure plasma treatment. This allowed determination of the joint performance and identification of the current limits of the 3D-printed composite when its conditions are stressed in adhesive bonding.

The experimental findings confirmed the effectiveness of LPP treatment in increasing the Onyx-surface functionalities. This reflected in SLJ shear strength that was nearly three times higher than that of abraded samples. Nevertheless, this situation emphasized the susceptibility of the base material to delamination, since the treatment caused generation of interfacial conditions between adhesive and adherend that were more effective than the interlaminar ones within the substrate. Hence, the performance limit of the adhesive system is established by the intrinsic non-homogeneity of the as-printed base material. Indeed, failure analysis pointed out that the crack planes corresponded to specific printed layers, precisely positioned at the interface between the two materials or just within the Onyx shell, where interlayer bonding appears to be weakened by the presence of gaps having an extent of several micrometers.

The results of this preliminary study have been considered informative to recognize possible methods to overcome the limitations highlighted, now subject of investigation by the authors. Notably, the use of more ductile adhesives, as well as adhesive-modulus tailoring methods, might be preferred ways to reduce stress concentrations at joint edges. In parallel, the adoption of post-printing hot-press or autoclave cycles is recognized as a promising method to maximize interlaminar bonding performance and reduce the extent of material discontinuities in the bulk.

Declaration of competing interest

The authors declare that they have no known competing financial interests or personal relationships that could have appeared to influence the work reported in this paper.

Acknowledgments

The authors acknowledge prof. Carla Gambaro and her staff at the Department of Mechanical Engineering of the University of Genoa for valuable insights on experiment planning, mechanical testing and data interpretation; Andrea Furlan is acknowledged for his technical support.

The authors also acknowledge the staff of Istituto Italiano di Tecnologia (IIT). In particular, sincere thanks goes to Riccardo Carzino (Smart Materials) and Dr. Marco Salerno (Materials Characterization Facility) for their valuable support in the wettability and morphological appraisals, respectively, and to Dr. Marco Maggiali (iCub Tech Facility) for helpful discussions.

References

[1] Parandoush P, Lin D. A review on additive manufacturing of polymer-fiber composites. Compos Struct 2017;182:36–53. https://doi.org/10.1016/j.compstruct.2017.08.088.
[2] Tekinalp HL, Kunc V, Velez-Garcia GM, Duty CE, Love LJ, Naskar AK, et al. Highly oriented carbon fiber-polymer composites via additive manufacturing. Compos Sci Technol 2014;105:144–50. https://doi.org/10.1016/j.compscitech.2014.10.009.
[3] Zhong W, Li F, Zhang Z, Song L, Li Z. Short fiber reinforced composites for fused deposition modeling. Mater Sci Eng A 2001;301:125–30. https://doi.org/10.1016/S0921-5093(00)01810-4.
[4] Pidcock GC, het Panhuis M. Extrusion printing: extrusion printing of flexible electrically conducting carbon nanotube networks. Adv Funct Mater 2012;22:4789. https://doi.org/10.1002/adfm.201290133 (Adv. Funct. Mater. 22/2012).
[5] Dickson AN, Barry JN, McDonnell KA, Dowling DP. Fabrication of continuous carbon, glass and Kevlar fibre reinforced polymer composites using additive manufacturing. Addit Manuf 2017;16:146–52. https://doi.org/10.1016/j.addma.2017.06.004.
[6] Mei H, Ali Z, Yan Y, Ali I, Cheng L. Influence of mixed isotropic fiber angles and hot press on the mechanical properties of 3D printed composites. Addit Manuf 2019;27:150–8. https://doi.org/10.1016/j.addma.2019.03.008.
[7] Kabir SMF, Mathur K, Seyam AFM. A critical review on 3D printed continuous fiber-reinforced composites: history, mechanism, materials and properties. Compos Struct 2020;232:111476. https://doi.org/10.1016/j.compstruct.2019.111476.
[8] Blok LG, Longana ML, Yu H, Woods BKS. An investigation into 3D printing of fibre reinforced thermoplastic composites. Addit Manuf 2018;22:176–86. https://doi.org/10.1016/j.addma.2018.04.039.
[9] Pyl L, Kalteremidou KA, Van Hemelrijck D. Exploration of specimen geometry and tab configuration for tensile testing exploiting the potential of 3D printing freeform shape continuous carbon fibre-reinforced nylon matrix composites. Polym Test 2018;71:318–28. https://doi.org/10.1016/j.polymertesting.2018.09.022.
[10] Wang X, Jiang M, Zhou Z, Gou J, Hui D. 3D printing of polymer matrix composites: a review and prospective. Compos B Eng 2017;110:442–58. https://doi.org/10.1016/j.compositesb.2016.11.034.
[11] Ye W, Lin G, Wu W, Geng P, Hu X, Gao Z, et al. Separated 3D printing of continuous carbon fiber reinforced thermoplastic polyimide. Compos Part A Appl Sci Manuf 2019;121:457–64. https://doi.org/10.1016/j.compositesa.2019.04.002.
[12] Goh GD, Dikshit V, Nagalingam AP, Goh GL, Agarwala S, Sing SL, et al. Characterization of mechanical properties and fracture mode of additively manufactured carbon fiber and glass fiber reinforced thermoplastics. Mater Des 2018;137:79–89. https://doi.org/10.1016/j.matdes.2017.10.021.
[13] El Moumen A, Tarfaoui M, Lafdi K. Modelling of the temperature and residual stress fields during 3D printing of polymer composites. Int J Adv Manuf Technol 2019;104:1661–76. https://doi.org/10.1007/s00170-019-03965-y.
[14] Pizzorni M, Lertora E, Mandolfino C. Low pressure plasma treatment of CFRP substrates for adhesive bonding : an investigation of joint durability under severe temperature-moisture conditioning. Int J Adhesion Adhes 2020;99:102592. https://doi.org/10.1016/j.ijadhadh.2020.102592.
[15] Pizzorni M, Lertora E, Gambaro C, Mandolfino C, Salerno M, Prato M. Low-pressure plasma treatment of CFRP substrates for epoxy-adhesive bonding: an investigation of the effect of various process gases. Int J Adv Manuf Technol 2019;102. https://doi.org/10.1007/s00170-019-03350-9.
[16] Ebnesajjad S. Material surface preparation techniques. Adhes Technol Handb 2009:37–46. https://doi.org/10.1016/b978-0-8155-1533-3.50006-2.
[17] Wegman RF, Van Twisk J. Surface preparation techniques for adhesive bonding. second ed. Elsevier; 2013. https://doi.org/10.1016/B978-1-4557-3126-8.00003-8.
[18] Iragi M, Pascual-González C, Esnaola A, Lopes CS, Aretxabaleta L. Ply and interlaminar behaviours of 3D printed continuous carbon fibre-reinforced thermoplastic laminates; effects of processing conditions and microstructure. Addit Manuf 2019;30:100884. https://doi.org/10.1016/j.addma.2019.100884.
[19] Caminero MA, Chacón JM, García-Moreno I, Reverte JM. Interlaminar bonding performance of 3D printed continuous fibre reinforced thermoplastic composites using fused deposition modelling. Polym Test 2018;68:415–23. https://doi.org/10.1016/j.polymertesting.2018.04.038.
[20] Frascio M, de Sousa Marques EA, Carbas RJC, da Silva LFM, Monti M, Avalle M. Review of tailoring methods for joints with additively manufactured adherends and adhesives. Materials (Basel) 2020;13. https://doi.org/10.3390/ma13183949.
[21] Frascio M, Mandolfino C, Moroni F, Jilich M, Lagazzo A, Pizzorni M, et al. Appraisal of surface preparation in adhesive bonding of additive manufactured substrates. Int J Adhesion Adhes 2021;106:102802. https://doi.org/10.1016/j.ijadhadh.2020.102802.
[22] Mandolfino C, Lertora E, Gambaro C, Pizzorni M. Functionalization of neutral polypropylene by using low pressure plasma treatment: effects on surface characteristics and adhesion properties. Polymers (Basel) 2019;11. https://doi.org/10.3390/polym11020202.
[23] Mandolfino C, Lertora E, Gambaro C, Pizzorni M. Durability of polyamide bonded joints: influence of surface pre-treatment. Int J Adhesion Adhes 2018;86:123–30. https://doi.org/10.1016/j.ijadhadh.2018.08.002.
[24] EN ISO 25178. Geometrical product specifications (GPS) — surface texture : areal Part 1 : indication of surface texture. 2016.
[25] ASTM D 1002-05. Standard test method for apparent shear strength of single-lap-joint adhesively bonded metal specimens by tension loading (Metal-to-Metal). Standards 2005:1–5. https://doi.org/10.1520/D1002-10.on.
[26] ASTM International. ASTM D3039 - Standard test method for tensile properties of polymer matrix composite materials. Annu Book ASTM Stand 2014. https://doi.org/10.1520/D3039.
[27] Mandolfino C, Lertora E, Gambaro C. Influence of cold plasma treatment parameters on the mechanical properties of polyamide homogeneous bonded joints. Surf Coating Technol 2017;313:222–9. https://doi.org/10.1016/j.surfcoat.2017.01.071.
[28] Karsli NG, Aytac A. Tensile and thermomechanical properties of short carbon fiber reinforced polyamide 6 composites. Compos B Eng 2013;51:270–5. https://doi.org/10.1016/j.compositesb.2013.03.023.
[29] Arikan E, Holtmannspötter J, Zimmer F, Hofmann T, Gudladt HJ. The role of chemical surface modification for structural adhesive bonding on polymers - washability of chemical functionalization without reducing adhesion. Int J Adhesion Adhes 2019;95:102409. https://doi.org/10.1016/j.ijadhadh.2019.102409.
[30] Cansoy CE, Erbil HY, Akar O, Akin T. Effect of pattern size and geometry on the use of Cassie-Baxter equation for superhydrophobic surfaces. Colloid Surf A Physicochem Eng Aspect 2011;386:116–24. https://doi.org/10.1016/j.colsurfa.2011.07.005.
[31] Shu Y, Ye L, Yang T. Study on the long-term thermal-oxidative aging behavior of polyamide 6. J Appl Polym Sci 2008;110:945–57. https://doi.org/10.1002/app.28647.
[32] Štěpánová V, Šrámková P, Sihelník S, Stupavská M, Jurmanová J, Kováčik D. The effect of ambient air plasma generated by coplanar and volume dielectric barrier discharge on the surface characteristics of polyamide foils. Vacuum 2021:183. https://doi.org/10.1016/j.vacuum.2020.109887.
[33] van de Werken N, Tekinalp H, Khanbolouki P, Ozcan S, Williams A, Tehrani M. Additively manufactured carbon fiber-reinforced composites: state of the art and perspective. Addit Manuf 2020;31:100962. https://doi.org/10.1016/j.addma.2019.100962.
[34] Kumar S, Wardle BL, Arif MF, Ubaid J. Stress reduction of 3D printed compliance-tailored multilayers. Adv Eng Mater 2018;20:1–8. https://doi.org/10.1002/adem.201700883.